

High-frequency measurements of interfacial friction using quartz crystal resonators integrated into a surface forces apparatus

Steffen Berg, Marina Ruths,* and Diethelm Johannsmann†

Max-Planck-Institute for Polymer Research, Ackermannweg 10, D-55128 Mainz, Germany

(Received 27 August 2001; published 18 January 2002)

A quartz crystal resonator covered with a thin sheet of mica was integrated into a surface forces apparatus. The shifts in resonance frequency and bandwidth were monitored as the mica surface came into contact with a spherical lens approached from above. We compare experiments where the lens was either coated with a second mica sheet or just had a silver layer evaporated onto its surface. For the contact with the silver surface, strong maxima in bandwidth occurred during the formation and the disruption of the contact. No such maxima were seen when approaching and separating two mica surfaces. We attribute this increased dissipation to sliding and rolling friction, involving plastic deformation of the metal surface under oscillatory load.

DOI: 10.1103/PhysRevE.65.026119

PACS number(s): 81.40.Pq

I. INTRODUCTION

Friction, albeit an everyday experience, is still poorly understood in terms of its underlying mechanisms [1]. Amontons' laws state that the friction force is proportional to the vertical load, but independent of both the contact area and the lateral speed. The independence of contact area and sliding speed contrasts strongly with liquidlike friction as given, for instance, by Stokes' law, which states that for a sphere immersed in a viscous liquid, the friction force is proportional to the speed and radius. Bowden and Tabor have argued that sliding friction as expressed in Amontons' laws is the result of multiasperity contacts [2], where the size of each contact is governed by the local yield stress. The true contact area (to be distinguished from the apparent macroscopic contact area) is then proportional to the vertical force. The force of sliding friction is proportional to the true contact area and, therefore, proportional to the vertical load. Since the local stresses at the point contacts are high, the material locally undergoes plastic deformation or even suffers from plastic instabilities. Although the microscopic behavior is expected to be complex, one can rationalize a strongly sublinear stress-speed relation by local plasticity: once the local yield stress is exceeded, the material deforms and the stress increases only weakly with strain.

The work of Bowden and Tabor has given rise to the field of "nanotribology" [3]. When the objects sliding across each other are either very small or very smooth, multiasperity contacts can be avoided and experiments on the fundamental mechanisms of sliding friction become possible. The instruments mostly employed for these studies are the friction force microscope (FFM) [4,5] and the surface forces apparatus (SFA) [6–8]. Quartz resonators were used for measurements of sliding of adsorbed layers of noble gases in the UHV [9,10]. In these experiments the layers slide under their

own inertia, which results in a rather weak shear stress. These experiments are conceptually different from the experiments described here. We report on the contact between a quartz resonator with a *second solid surface*.

As we have argued in previous publications [11,12], quartz crystals may have a special role in tribology. Because of their high oscillation frequency, they allow a positioning accuracy in the nanometer range and a high lateral speed (up to 1 m/s) at the same time. The "dynamic" SFA or the FFM usually do not reach such speeds, which are, on the other hand, frequently encountered in practical applications. The most prominent example, where sliding speeds beyond a meter per second and truly molecular distances are of importance, is the hard disk in a magnetic storage device [13]. High sliding speeds are encountered in most mechanical machines as well, although the lubricating films in these cases usually are thicker than a monolayer. In previous tribological experiments with quartz crystals, the sliding occurred between the (suitably modified) crystal surface and a macroscopic sphere [11,12] or the tip of an atomic force microscope (AFM) [14–16]. Such experiments lack absolute distance control and the capability of visual inspection of the contact area. In the following, we demonstrate how this can be achieved by incorporating a quartz crystal resonator into an interferometric SFA.

The SFA is a well-established instrument for measuring both normal and lateral interaction forces between two surfaces with subnanometer control of their relative distance [6,7,17]. In the standard SFA setup, a contact with a well-defined geometry is formed between atomically flat surfaces consisting of micrometer-thin mica pieces glued onto cylindrical supports that are mounted in a crossed geometry. The mica pieces have semitransparent silver layers on their back-sides, so that a pair of surfaces form an optical cavity that is used for interferometric distance measurements [18,19]. Such a setup has been used to study the static and dynamic forces in a large number of systems confined between smooth surfaces. At moderate loads, two bare mica surfaces can also be brought to slide past each other under dry conditions once the displacement exceeds a few micrometers [6].

Previous studies of friction of rough surfaces in the SFA

*Permanent address: Department of Physical Chemistry, Åbo Akademi University, Porthansgatan 3-5, FIN-20500 Åbo, Finland.

†Corresponding author. FAX: +49-6131-379 360. Email address: johannsmann@mpip-mainz.mpg.de

have concerned symmetrical systems of two identical silica [20] or alumina [21] surfaces with a roughness of about 0.2-nm rms, and silicon nitride [22] with a roughness of ca. 4-nm rms. For bare surfaces under dry conditions and loads of a few millinewton, the initiation of sliding typically requires a displacement in the micrometers range. The friction force for hydrophilic silica, alumina, and silicon nitride generally does not show the regular stick-slip behavior seen for atomically smooth surfaces. Instead, it shows small irregularities that reappear upon reversing the scan direction and reflect the multiasperity nature of the contact. Under dry conditions and slow sliding speeds (with sliding amplitudes of tens of micrometer), silica and alumina surfaces become damaged at loads of 10–20 mN.

We report on the integration of a quartz crystal resonator into an SFA in a manner that does not require significant modification of the SFA itself. Technical details are provided and results are given for two different systems, one with two bare mica surfaces coming into adhesive contact and another with one mica and one rough silver surface. We find fundamental differences in the responses of these two systems, and discuss these in terms of the contributions of friction and plastic deformation to the measured signals.

II. EXPERIMENTAL SETUP

Quartz crystals with a diameter of 14 mm and a fundamental resonance frequency of either 4 or 10 MHz were used as the lower surface in the SFA. Both surfaces of the quartz blank were planar. To allow the white light needed for the interferometry to pass through the setup, the electrode on the backside (lower side) of the crystal was keyhole shaped with a central hole with a diameter of 2 mm [Fig. 1(a)]. To still obtain an efficient confinement of the oscillation to the central portion of the quartz crystal (“energy trapping”), the rest of the back electrode had to be thicker than usual. Energy trapping is based on the fact that the resonator is thicker in the middle of the plate than at the rim. This can be achieved with keyhole shaped back electrodes alone, provided they are thick enough. The back electrode in the present experiments consisted of thermally evaporated silver (Unaxis, purity 99.99%) with a thickness of 750 nm. The front electrode, which also forms one of the reflecting surfaces in the interferometer, was a semitransparent silver layer with a thickness of 52 nm, evaporated onto the whole frontside of the quartz crystal. Onto the front electrode, we glued circular (diameter 5 mm) pieces of mica (S&J Trading, Glen Oaks, NY) that had been cut from larger pieces with a die cutter [23]. A small droplet (about 0.1 μl) of UV-curable glue (Norland Optical Adhesive 83H) was placed on the center of the front electrode. When a mica piece was placed on the glue, the droplet spread into the entire gap under the piece due to capillary forces. The glue was cured by a 2-min irradiation with a mercury arc lamp (100 W). It is essential that the mica circles used for gluing are thick enough ($>10 \mu\text{m}$) to resist wrinkling induced by the capillary forces from the glue. The thickness can be decreased *after* gluing by cleaving with adhesive tape. The complete assembly, mounted in its holder, is shown in Fig. 1(b). The rather simple adapter for mounting

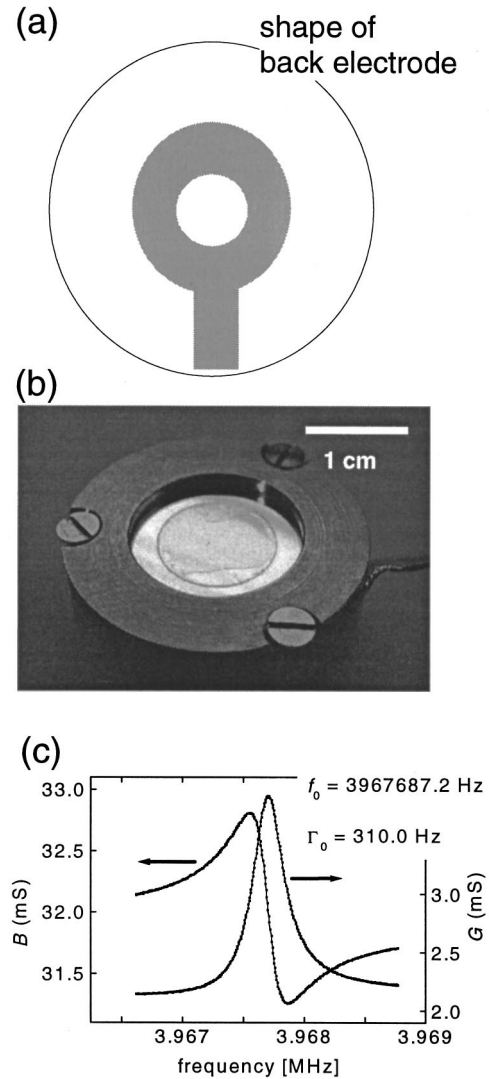


FIG. 1. Integration of a quartz crystal into the surface forces apparatus. (a) The keyhole-shaped silver electrode on the lower side of the quartz has a hole in the middle to allow the light necessary for optical measurements of distance to pass through. (b) A circular piece of mica has been glued to the front electrode in order to obtain an atomically flat surface. The quartz plate with the mica is placed in an adapter that can be mounted as the lower surface in the SFA. The adapter also supplies the electrical connection. Part (c) shows a trace of a resonance for a quartz plate with an attached mica circle as shown in (b). The conductance G and the susceptance B are the real and the imaginary part of the electrical admittance.

the quartz crystal on top of the lens holder for the lower surface in the SFA was made of brass. A ring of a rigid polymer (“Delrin”) was inserted below the quartz plate in order to provide electrical insulation between the lower electrode and the SFA lens holder [cf. Fig. 3(c)]. The cables connecting the electrodes to the impedance analyzer (not shown) were taken through a hole in an existing side plate of the instrument.

Typically, the glue-and-mica overlayer initially increased the resonance bandwidth by a factor of about 100. Most of this increase is caused by the mica, as is proven by the fact that the bandwidth gradually reverts toward its original value

when most of the mica is cleaved off successively with adhesive tape. The final, combined thickness of the glue-and-mica layer was estimated from optical measurements in each experiment and was typically 3–6 μm . In order to achieve a small bandwidth, which is important for an accurate determination of resonance frequency, it is critical that the edges of the mica are smooth and adhere well to the front electrode. Frayed out edges were the most common source of increased bandwidth (and can, later on, be a source of undesired side contacts with the upper surface). The type of the glue and its thickness appear to be less critical. A bandwidth of less than 1 kHz could be reached after cleaving of the mica. (Uncoated quartz blanks typically have bandwidths in the range of 50 Hz.) An example of the typical fundamental resonance obtained for a mica-coated quartz crystal is shown in Fig. 1(c). The resonance is slightly asymmetric and the conductance G is offset from zero by about 2 mS. This is indicative of imperfect calibration of the impedance analyzer. Since the fit routine accounts for such imperfections, the frequency determination is unaffected by these shortcomings. The drive power was typically -10 dBm (where 0 dBm corresponds to 1-mW electrical power). Although, in principle, much higher drive levels (and as a consequence much higher lateral speeds) can be chosen, this low power ensures a resonance frequency independent of the drive level. At higher drive levels, the quartz becomes intrinsically nonlinear, mostly caused by heating due to internal friction. At the drive level chosen here the amplitude of lateral motion and the lateral speed are ~ 0.7 nm and 15 mm/s, respectively [24].

Usually, only the fundamental resonance peak showed a thickness shear mode that was well separated from the anharmonic sidebands. On the overtones, the anharmonic sidebands overlapped with the main resonance. Presumably, unevenness in the glue layer or the rather peculiar form of the back electrode spoiled the mode structure. Because the natural length scale in acoustic experiments is the wavelength of sound, imperfections are more detrimental at higher frequencies. For the same reason, experiments with quartz crystals with a resonance frequency of 4 MHz were easier than experiments with 10 MHz crystals.

The frequency-dependent complex admittance $Y = G + iB$ was fitted with the functions

$$G_{\text{fit}} = G_{\text{max}} \left[\frac{f^2 (2\Gamma)^2}{(f_0^2 - f^2)^2 + (2\Gamma)^2 f^2} \cos \varphi - \frac{(f_0^2 - f^2)}{(f_0^2 - f^2)^2 + (2\Gamma)^2 f^2} \sin \varphi \right] + G_{\text{off}}, \quad (1a)$$

$$B_{\text{fit}} = G_{\text{max}} \left[-\frac{(2\Gamma)^2 f^2}{(f_0^2 - f^2)^2 + (2\Gamma)^2 f^2} \sin \varphi - \frac{(f_0^2 - f^2)}{(f_0^2 - f^2)^2 + (2\Gamma)^2 f^2} \cos \varphi \right] + B_{\text{off}}, \quad (1b)$$

where G_{max} is an amplitude, f_0 is the resonance frequency, Γ is the half-band-half (HBH) width, φ is an asymmetry parameter, and G_{off} and B_{off} are offsets. Usually, the fit quality

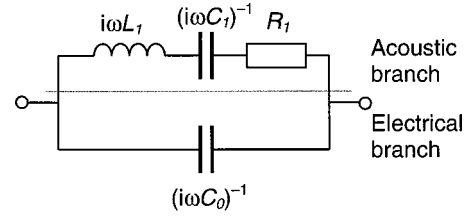


FIG. 2. The Butterworth-van Dyke (BvD) equivalent circuit has three acoustic elements, which are the motional inductance L_1 , the motional capacitance C_1 , and the motional resistance R_1 .

is such that the fit can be hardly distinguished from the data [cf. Fig. 1(c)]. The asymmetry parameter φ was introduced to account for a rotation of the resonance curve in the complex plane (polar diagram). Such an asymmetry is clearly visible in Fig. 1(c) (particularly in the conductance trace, which is asymmetric). While the most important parameters for interpretation are the frequency f_0 and the HBH width Γ , the other parameters (in particular, the amplitude, G_{max}) may carry information, as well.

Generally speaking, all parameters not based on frequency have to be interpreted with care because they are much more susceptible to electrical artifacts than the frequencies. Calibration is another problem. Since the quartz is at a rather remote location, calibration with known resistors at the exact same place is difficult and was not attempted here. The derived frequencies and bandwidths are unaffected by calibration. Offsets and asymmetry, however, do depend on calibration and we are not surprised to find them rather sizable. The fact that offset and asymmetry change when contact is being formed may be ascribed to the changing electrical boundary conditions. The amplitude G_{max} , on the other hand, primarily is an acoustic quantity, although it is measured by electrical means and, therefore, contaminated with electrical disturbances. The physical interpretation of the parameter G_{max} is based on the Butterworth-van Dyke (BvD) equivalent circuit shown in Fig. 2. The BvD circuit contains three acoustic elements that are the motional inductance, L_1 (equal to $M_q/2$, with M_q the mass of the active portion of the quartz [25]), the motional capacitance C_1 (equal to $2d_q/[\pi^2 S G_q (1 - \kappa^2)]$, with d_q the thickness of the resonator, S the active area, G_q the shear modulus, and $\kappa^2 = 0.008$ the piezoelectric coupling constant [25]), and a motional resistance R_1 (related to viscous dissipation). All three parameters can be derived separately via the relations

$$2\pi f_0 = \frac{1}{\sqrt{L_1 C_1}},$$

$$Q = \frac{f_0}{2\Gamma} = \left(\frac{L_1}{C_1} \right)^{1/2} \frac{1}{R_1}, \quad (2)$$

$$G_{\text{max}} = \frac{\phi^2}{S} \left(\frac{L_1}{C_1} \right)^{1/2}$$

with Q the Q factor, and $\phi = S e'_{26} / d_q$ a factor that converts from acoustic to electrical impedance. $e'_{26} = 9.65 \times 10^{-2} \text{ Cm}^{-2}$ is the piezoelectric coefficient. In abso-

lute terms, G_{\max} can serve to estimate the active area of the quartz plate S , since this quantity enters the conversion from acoustic to electric impedance. When G_{\max} varies this may be ascribed to changes in either the active area or in changes in L_1/C_1 . Assuming that the active area remains constant, one can use Eq. (2) to derive L_1 , C_1 , and R_1 from the resonance parameters. For a bare quartz plate one expects that $(L_1/C_1)^{1/2} = \pi/2Z_q$. The “normalized impedance” shown in Figs. 5 and 7 in the results section is equal to $(L_1/C_1)^{1/2}/(\pi/2Z_q)$. In the derivation, we assumed that the active area was a circular disc with an equivalent radius of 3.5 mm. Given that the normalized impedance is found to be close to one, this seems to have been a reasonable choice. The emphasis in Figs. 5 and 7 is on the *variation* of the normalized impedance, not on its absolute value.

As the opposing surface we used plane-convex lenses (Newport, Darmstadt, Germany) with a diameter of 10 mm and a radius of curvature of either 7.8 or 10.4 mm. The curved surface of the lens was either covered with an evaporated layer of silver (thickness 52 nm) [Fig. 3(a)] or with a small piece of back-silvered mica [Fig. 3(b)]. In the first case, the surface roughness of the silver layer was around 4-nm rms (15 nm peak-to-peak) as determined with AFM over an area of $25\mu\text{m}^2$. The second case enabled us to investigate also the contact between two atomically smooth surfaces in a plate-sphere geometry. It is indeed possible to glue a small piece of thin mica (size ca. 3×3 mm, thickness $< 2 \mu\text{m}$) onto a spherical support, provided that one uses a liquid glue (in this case a molten 1:1 mixture of galactose and dextrose), so that one can control the positions of unavoidable folds in the mica extending radially from the highest point of the glue droplet. The mica piece is possibly able to comply with a small amount of biaxial curvature. With some practice, one can obtain a surface with a softly curved top that gives a single, circular or slightly elliptical contact with a flat surface. The radius of curvature of such a contact position is typically 1–3 cm, which is similar to the one obtained in standard SFA experiments with two crossed, cylindrical surfaces.

The half-spherical lens was placed in the standard holder for the upper surface so that it faced the lower surface (the mica-coated quartz) [Figs. 3(c) and 3(d)]. The distance between the surfaces, and thus the pressure in contact, was regulated with the standard motor-driven micrometer controls of the SFA. The spring constant of the spring supporting the lower surface (cf. Figs. 3(c) and 3(d)) was 520 N/m, giving a sensitivity in the measurement of normal forces of about 10^{-7} N.

The distance between the surfaces was determined by multiple beam interferometry. The fringes of equal chromatic order had the appearance expected for a two-layer [18] or asymmetric [19] interferometer, depending on the system. We could always observe birefringence, also in the experiments involving only one mica sheet, which was an indication that mica was indeed left on the lower surface after cleaving with tape.

In experiments with an evaporated silver layer on the top lens, the interferometer can be very thin (occasionally only 1–2 μm), and one can see some larger-scale roughness (un-

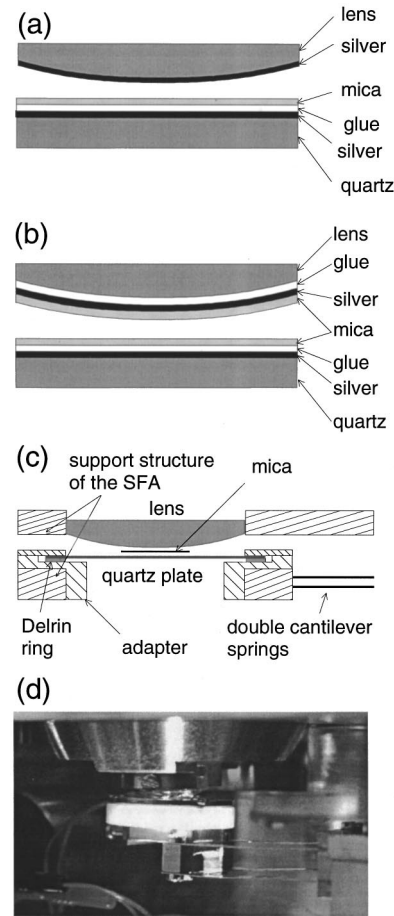


FIG. 3. Schematic drawings (a,b) of the two systems studied: The front electrode of the quartz was always coated with a mica sheet as shown in Fig. 1(b). The opposing lens was either covered with an evaporated 52-nm-thick silver layer (a) or with a back-silvered mica sheet (b). Panel (c) shows a sketch of the experimental setup. The adapter with the quartz plate and the lens are inserted in the holders, where conventionally the fused silica cylinders of a standard SFA are mounted. Panel (d) shows a photograph of the assembly inside the SFA.

dulations with a height of a few nanometers) on the fringe. (Recalling that in the optical measurement, the resolution in the surface plane is about 1 μm , this shows the variations in the average height of the evaporated silver layers over a length scale of a few micrometers). In this system, the closest distance between the surfaces at hard compression with the coarser motor control (a normal force of 5–10 mN) was taken as zero distance. The high compression used to define “zero” causes both plastic deformation of asperities of the metal layer (which will be discussed below) and some elastic deformation of the glue layer. The interferometer was approximated by a two-layer system, where one layer was taken as the glue (refractive index 1.56) together with the mica, and the other layer was assumed to be air (ignoring the presence of silver “spikes” that occupy a small fraction of the air volume [26] as the rough silver surface first touches the mica). Since we were mainly interested in *changes* in distance when the surfaces come in contact, this approximation was used together with a simplified equation for a two-

layer interferometer [18], valid only at small separations. Clean surfaces generally came into first contact at a separation distance of about 11–17 nm from the defined “zero” at high compression (cf. Fig. 6(c) in the results section), which is in good agreement with the measured peak-to-peak roughness of the silver layer. The “air gap” could be compressed stepwise with the sensitive motor control by about 7–10 nm, which is likely a compression and flattening of the peaks of the rough silver layer. The compression thus constitutes an increase in the true contact area, even though the macroscopic shape of the reflecting layers did not change (both were evaporated on rigid substrates), and a change in the width (lateral dimension) of the silver peaks cannot be resolved optically. After compression, a strong adhesion and even some extension could be seen on separation. Generally, the surfaces would come back to the original contact and onset of forces (around 15 nm from the defined “zero”) on a new approach. Occasionally the surfaces were damaged on separation, which resulted in a longer-ranged repulsion (upon the observation of such changes in the forces on approach, the experiment was discontinued).

In the case of two mica pieces facing each other, the surfaces spontaneously jumped into contact due to van der Waals forces, as is normally seen for clean mica surfaces. This strongly adhesive contact in dry air defined zero distance in the mica-mica system. The contact area could be directly measured from the shape of the flattened tip of the fringe, since now the upper, back-silvered mica piece was supported on a deformable glue [cf. Fig. 3(b)]. As expected, the mica surfaces could be approached and separated several times without damage or changes in distance.

In these preliminary experiments, the glue on the quartz is situated inside the optical cavity. Since the glue varies in thickness over the sample area, this complicates the analysis of distances with respect to the defined zero distance in cases where new contact positions have to be found, and the refractive index of the glue does not exactly match that of the mica as assumed in the distance calculation above. In future experiments, we intend to use back-silvered mica also on the quartz, so that the optical cavity would contain only the mica and the sample of interest, and also large separation distances could be calculated in the standard manner [18,19]. The front electrode on the quartz must then have a hole like the back electrode in order to provide optical accessibility.

All experiments were done at room temperature and atmospheric pressure. The instrument chamber was purged with dried nitrogen (<5% humidity) for about one hour prior to the experiment. During the experiment, the purging was stopped, and a vessel with phosphorous pentoxide was placed in the chamber to take up humidity.

III. RESULTS AND DISCUSSION

The majority of our initial attempts were unsuccessful as a result of contamination, mainly by small dust particles whose presence could be inferred from long-range repulsion observed as the surfaces were brought close, and seen as deformations on the interference fringe pattern as the sur-

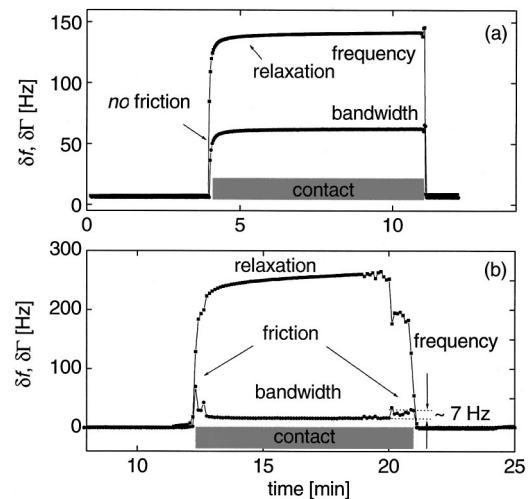


FIG. 4. (a) Shifts in frequency and bandwidth upon touching the mica on the quartz plate with a second mica surface in dry air. Since the surfaces jumped spontaneously into contact from a close distance, the rate of approach was not controlled. No external load was applied. The frequency of oscillation was 4 MHz. (b) Shifts in frequency and bandwidth upon touching the mica on the quartz plate with a bare silver surface in dry air. The surfaces drifted into contact at a rate of about 0.1–0.5 nm/s and reached a maximum load of < 0.5 mN.

faces came in contact. The particles might to some extent appear when cleaving the mica on the quartz with tape, especially if larger steps are created across the surface, but could also come from occasional exposure of the quartz assembly to the laboratory air during initial calibration procedures. The silvered top surface (lens) might become contaminated when removing it from the evaporator. Handling of the quartz crystals in a laminar flow cabinet, as we normally did for other procedures involving the SFA (including the gluing of mica on the top lens) greatly reduced this problem. The occurrence and identification of contamination illustrates how important it is to have optical access to the contact zone.

In Fig. 4, we compare the signals from the quartz crystal when contact is being made between the lower mica surface (on the quartz) and a mica surface glued onto the top lens [cf. Fig. 3(b)], and between the lower mica surface and a silvered lens [cf. Fig. 3(a)]. The contact is subsequently being released after a contact time of about 5 min. The results of the two experiments are strikingly different. For the contact between the mica and the silver there is a strong maximum in the bandwidth when the contact is just being established. It will be shown below that this point coincides with the onset of normal interactions between the surfaces. This maximum is absent for the contact between two pieces of mica, where the surfaces spontaneously jumped into an instantaneous contact over an area of about $4 \times 10^{-10} \text{ m}^2$ due to van der Waals forces. In the mica-silver system, some further changes in the frequency shift after the initial contact can be ascribed to a combined effect of relaxation in the glue (on the quartz) and of silver deformation. When the two mica pieces are in adhesive contact, there is also some relaxation (likely in the two supporting glue layers), although smaller

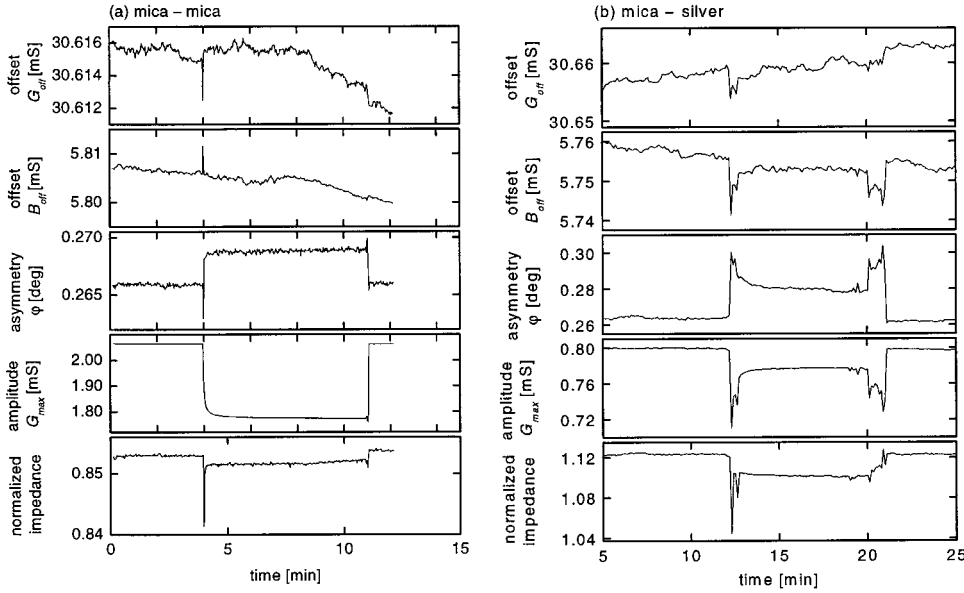


FIG. 5. Fit parameters other than frequency and bandwidth for the data from Fig. 4. See the Experimental section for the definition of the parameters. Note that the normalized impedance behaves differently on approach and separation.

than in the mica-silver system. The relaxation is consistent with a slight increase in contact area observed from the fringe pattern arising from the mica-mica contact during this time.

Upon separation of the surfaces, a similar maximum in the bandwidth as on approach is seen for the mica-silver contact. For the mica-mica contact, there is an indication of a small maximum. The separation of two mica surfaces normally follows the so-called Johnson, Kendall, and Roberts (JKR) theory [27,28] and thus occurs from a finite contact area with a radius of about 60% of the one on initial contact at zero load (where no maximum was seen). Possibly the backlash present in the mechanical controls could have induced a slight increase in pressure at the initiation of separation, which could be seen as an increase in the signals that is not caused by friction.

Figure 5 shows the fit parameters not related to frequency for the data from Fig. 4. These are the offsets of the conductance and the susceptance, a phase parameter quantifying the asymmetry of the resonance [cf. Fig. 1(c)], and the resonance amplitude G_{\max} . In the bottom panel a normalized impedance has been derived from G_{\max} and the Q factor as described in the experimental section. As stated above, the electrical parameters have to be interpreted with care. We do, however, observe systematic effects. In particular, the normalized impedance shows a negative peak on approach but no such anomaly on separation.

In Fig. 6, we show data for a contact between mica and silver where the distance has been changed in small steps. Figs. 6(c) and 6(d) show the force between the surfaces in the normal direction vs the optically measured distance (as defined in the experimental section), and the frequency shift vs the normal force, respectively. As mentioned previously, there is a substantial adhesion hysteresis and some extension upon separation. In contrast to systems of elastically deforming rough surfaces, which are expected to show low adhesion [29], the strong adhesion and extension of our mica-metal contact on separation suggest that some of the silver, likely the highest points on the rough surface, becomes plastically

deformed after an external pressure has been applied. Flattening of a rough silver layer against mica after long contact times and adhesion of similar magnitude as in our experiment have also been observed by others [30]. Especially at high compression, there might be some small elastic deformation of the glue layer under the mica, but this cannot be the cause for the adhesion hysteresis and shear responses seen during the compression and separation.

When comparing Figs. 4(a), 4(b), 6(a), and 6(b), one notices a large difference in the absolute change of the bandwidth. We attribute this to differences in the contact area and normal load. In Fig. 4(a), the actual contact area is very large compared to in Figs. 4(a) and 6, because of the smoothness of the two mica surfaces. In Fig. 6, we increased the normal force stepwise with the surfaces in contact, whereas in Fig. 4(b) the surfaces just drifted into first contact. Therefore, the real contact area (flattened asperities) is larger in Fig. 6 than in Fig. 4(b), but still smaller than in Fig. 4(a). Based on an argument raised by Borovski and co-workers [1], one can also analyze the ratio between the HBH width shift $\delta\Gamma$ and frequency shift δf in terms of multiasperity contacts. Disregarding sliding or rolling friction, the simple contact mechanical model from Ref. [11] states that this ratio should be equal to kr_c , with k the wave number of sound and r_c the contact radius. A small ratio of $\delta\Gamma/\delta f$ [as found in Fig. 4(b)] suggests that the contact is made across a multitude of small contacts, all of them having a small radius r_c .

The main peaks in the bandwidth occur when the quartz plate first touches and when the surfaces finally separate. However, there are also smaller maxima when the lower stage is moved. After each step (compression or separation) there is relaxation, evidenced by a gradual change in frequency shift. Figure 7 shows the remaining fit parameters for the data from Fig. 6. Again, the normalized impedance behaves differently for approach and separation.

Clearly the peaks in bandwidths seen on approach and separation of the mica to the silver should be ascribed to dissipative processes. The interpretation can be based on two distinct processes, which are sliding friction [1] and rolling

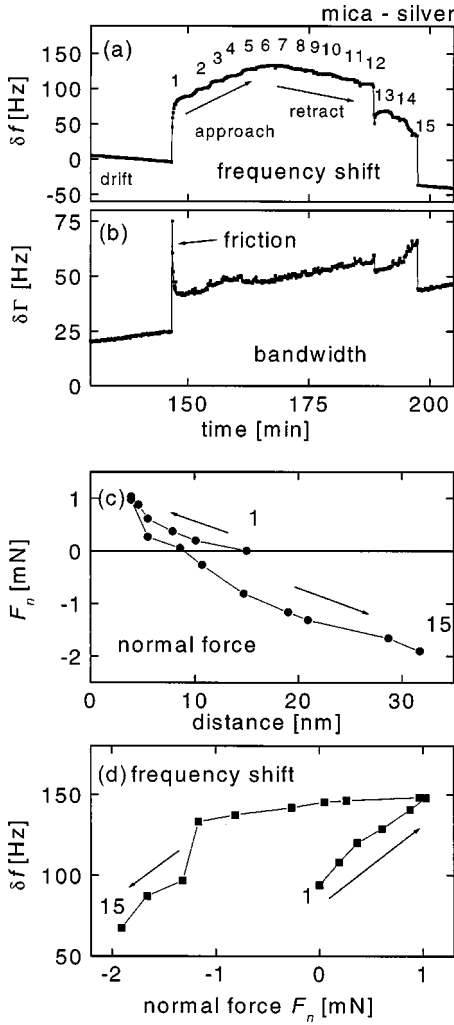


FIG. 6. Contact between mica and silver. Traces of (a) frequency shift and (b) bandwidth as a function of time for a series of steplike movements of the lower stage. Points 1–6 represent increasing compressions and 7–15 separations. Panel (c) shows the normal force vs the optically measured distance. Generally, no force was observed until the surfaces came to a separation of about 15 nm from the defined closest separation (as defined in the text), where a monotonically repulsive force appeared. Occasionally, a small jump inward to this same distance occurred. In both cases, the onset of the repulsive force coincided with the increase in frequency shift and bandwidth. There is a strong adhesion hysteresis. Panel (d) shows the frequency shift vs normal force, again demonstrating the strong hysteresis.

friction [31,32]. Here, we understand sliding and rolling friction as two different phenomena that may be caused by a variety of different elementary processes. Sliding friction is discussed in many textbooks [1,2,13]. The elementary processes of rolling friction are less clear. Plastic deformation is most probably one of them [33]. In the following, we argue that rolling friction must be part of the explanation.

Using the JKR model and some reasonable numbers, we find that the vertical pressure in the center of the contact region is about 10^7 Pa even at zero external force [34]. The contact radius at zero-external force r_c is about 20 μm ,

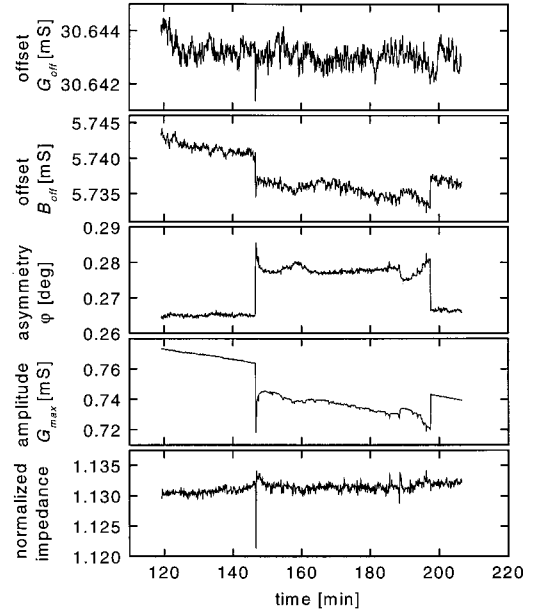


FIG. 7. Fit parameters other than frequency and bandwidth for the data from Fig. 6. See the Experimental section for the definition of the parameters. As in Fig. 5, the normalized impedance behaves differently on approach and separation.

which is consistent with observations. Our analysis aims only for an order of magnitude estimate and ignores the fact that the true contact area has a complicated shape due to the initial surface roughness, which is reduced by plastic deformation [26,30]. The amplitude of motion, u , is about 1 nm. It seems highly unlikely that such a small amplitude could cause sliding once the surfaces are in adhesive contact. One can estimate the interfacial shear stress σ from the frequency shift δf as [35]

$$\begin{aligned} \sigma &= \pi Z_q \frac{S}{A_c} \frac{\delta f}{f_0} \frac{du}{dt} = \pi Z_q \frac{S}{A_c} 2\pi \delta f u \\ &= 2\pi^2 Z_q \frac{S}{A_c} \delta f Q \frac{2}{\pi} \frac{d_{26} U_{el}}{2} = 2\pi Z_q \frac{S}{A_c} \delta f Q d_{26} U_{el}, \end{aligned} \quad (3)$$

where $Z_q = 8.8 \cdot 10^6 \text{ kg}/(\text{m}^2 \text{ s})$ is the acoustic impedance of AT-cut quartz, $\delta f \sim 200 \text{ Hz}$ is the frequency shift, f_0 is the frequency of the fundamental, u is the lateral displacement, $S \sim 0.7 \text{ cm}^2$ is the active area of oscillation, which roughly corresponds to the area under the back electrode, $A_c \sim \pi r_c^2$ is the contact area (cf. discussion above), $Q = f_0/(2\Gamma)$ is the Q factor, $d_{26} = 3.1 \text{ pm}/\text{V}$ is the piezoelectric coefficient, and $U_{el} = 100 \text{ mV}$ is the electrical voltage across the electrodes. Note that we have averaged the shear stress over the entire contact area. Inserting values, one finds a shear stress of only 10^6 Pa , which is below the yield stress, the latter being much above 1 MPa. We expect that the shear stress would be much lower than the yield stress in refined models as well (taking, for instance, roughness and a nonuniform stress distribution into account).

While we cannot exclude that some sliding friction occurs when contact is being made, we find that (based on the previous arguments) sliding friction cannot account for the increased bandwidth upon *separation*. This leaves rolling friction as the likely explanation [31]. The term “rolling friction” here denotes all processes of dissipation connected to a rolling or tilting motion, regardless of the underlying elementary processes. We see two distinct fundamental processes that are (a) adhesion hysteresis and (b) plastic deformation of the subsurface region [36]. Adhesion hysteresis can arise due to energy conversion into heat or sound upon contact formation. This energy is irreversibly lost. The dissipation caused by adhesion hysteresis should be less than the surface energy times the frequency. Below, we test this prediction by comparing the experimentally observed total dissipated power with the surface energy. The experimentally observed total dissipated power P_{tot} is $P_{\text{tot}} = U_{\text{el}}^2 G_{\text{max}} = (100 \text{ mV})^2 \times 0.8 \text{ mS} = 8 \mu\text{W}$. Of this total power, a fraction $\delta\Gamma_{\text{fric}}/\Gamma_{\text{tot}} = (7 \text{ Hz})/(345 \text{ Hz}) = 2\%$ is spent on friction, which gives a power dissipated in friction of $P_{\text{fric}} \sim 0.16 \mu\text{W}$ [see Fig. 4(b)]. The dissipated power due to adhesion hysteresis can be estimated using simple arguments on rolling friction along the lines of Ref. [33]. We assume that adhesion hysteresis (AH) occurs on a strip of the surfaces that undergoes adhesion-separation cycles under the shearing motion of the quartz. The width of this strip ξ_{AH} should not exceed the amplitude of the shear motion, which is of the order of 1 nm. The total dissipated power is $P_{\text{fric}} \cong A_{\text{AH}} G_{\text{AH}} f \cong 1/2 (2\pi r_c) \xi_{\text{AH}} G_{\text{AH}} f$, where $A_{\text{AH}} = 1/2 (2\pi r_c) \xi_{\text{AH}}$ is the area undergoing adhesion-separation cycles, G_{AH} is the energy dissipated per cycle and unit area, and f is the frequency. The factor of 1/2 was inserted because the area in question consists of two half moons, rather than a ring. Assuming that ξ_{AH} is less than 1 nm, one arrives at a lower boundary for G_{AH} of $G_{\text{AH}} > 1 \text{ J/m}^2$. This is much higher than what we expect for the equilibrium surface energy. Although the possibility of contamination prevents us from providing an exact number for the surface energy, a typical value would be in the range of 30–100 mJ/m². Our estimate shows that adhesion hysteresis alone cannot account for the amount of dissipation experimentally observed. Subsurface *plastic deformation* of the metal, therefore, contributes to the signal assumed to arise from friction. Plastic deformation also provides an explanation why “friction” should increase immediately before separation. Prolonged cycles of adhesion and separation will presumably deform the contact line until it comes to rest at pinning centers. These pinning centers would then reduce the oscillatory mo-

tion of the contact line and, concomitantly, reduce rolling friction. When the contact line is forced to move (for instance, by pulling back the mica surface) these pinning sites are lost.

We have limited our discussion to the increased friction on *separation* because true sliding friction might contribute to the friction when contact is being made. Interestingly, the normalized impedance behaves differently upon approach and separation [Figs. 5(e) and 7(e)]. At this point, we do not have a quantitative understanding of the variation of this parameter with the experimental conditions. We cannot exclude that the variation of the normalized impedance is connected to deviations of the resonance curves from Lorentzians [cf. Eq. (1)]. Should the stress-strain ratio or the friction coefficient be a function of amplitude, that is, should nonlinearities be present, the shape the resonance would be modified. Evidence for such nonlinear processes connected to friction has been gathered in ring-down experiments [37] and will be described in more detail in a separate publication. Nonlinear behavior is very common in friction phenomena. Despite this uncertainty in the quantitative aspects, we find the distinct asymmetry in the response on approach and separation interesting. Possibly sliding friction and rolling friction could be distinguished based on the normalized impedance.

IV. CONCLUSIONS

By combining a quartz crystal resonator with a surface forces apparatus, we have performed friction measurements under oscillatory movement at shear rates of up to 10 mm/s. The shape and cleanliness of the contact position was deduced from the optical interference pattern and the measured normal interaction force between the surfaces. There is a striking difference in the signal from the oscillating quartz crystal for the contact between two strongly adhering, atomically smooth mica sheets and between a mica sheet and a rough silver surface. Upon the formation and the disruption of the mica-silver contact there is a strong maximum in bandwidth, which we attribute to interfacial friction. The enhanced friction seen right before separation of the surface is attributed to rolling friction and plastic deformation of the metal surface.

ACKNOWLEDGMENTS

Part of this work was funded by the DAAD and the Academy of Finland in the frame of their program for bilateral exchange of researchers.

-
- [1] B. N. J. Persson, *Sliding Friction* (Springer, Heidelberg, 1998).
 [2] F. P. Bowden and D. Tabor, *Friction and Lubrication* (Methuen, London, 1967).
 [3] J. Krim, *Sci. Am.* **275**, 74 (1996).
 [4] G. M. McClelland, in *Adhesion and Friction*, edited by M. Grunze and H. J. Kreuzer, Springer Series in Surface Science, Vol. 17 (Springer, New York, 1989), p. 1.
 [5] E. Meyer, R. M. Overney, and J. Frommer, in *Handbook of Micro/Nano Tribology*, edited by B. Bushan (CRC, Boca Raton, 1995), p. 223.
 [6] A. M. Homola, J. N. Israelachvili, M. L. Dee, and P. M. McGuiggan, *J. Tribol.* **111**, 675 (1989); A. M. Homola, J. N. Israelachvili, P. M. McGuiggan, and M. L. Lee, *Wear* **136**, 65 (1990).

- [7] E. Kumacheva, *Prog. Surf. Sci.* **58**, 75 (1998).
- [8] J. N. Israelachvili, in *Handbook of Micro/Nano Tribology*, edited by B. Bushan (CRC, Boca Raton, 1995), p. 267.
- [9] J. Krim, D. H. Solina, and R. Chiarello, *Phys. Rev. Lett.* **66**, 181 (1991).
- [10] C. Mak, and J. Krim, *Phys. Rev. B* **58**, 5157 (1998).
- [11] A. Laschitsch and D. Johannsmann, *J. Appl. Phys.* **85**, 3759 (1999).
- [12] A. Laschitsch, L. E. Bailey, G. W. Tyndall, C. W. Frank, and D. Johannsmann, *Appl. Phys. Lett.* **78**, 2601 (2001).
- [13] B. Bushan, in *Handbook of Micro/Nano Tribology* edited by B. Bushan (CRC, Boca Raton, 1995), p. 443.
- [14] B. Borovsky, B. L. Mason, and J. Krim, *J. Appl. Phys.* **88**, 4017 (2000).
- [15] J. M. Kim, S. M. Chang, and H. Muramatsu, *Appl. Phys. Lett.* **74**, 466 (1999).
- [16] A. Sasaki, A. Katsumata, F. Iwata, and H. Aoyama, *Jpn. J. Appl. Phys., Part 2* **33**, L547 (1994).
- [17] J. N. Israelachvili, *Intermolecular and Surface Forces*, 2nd ed. (Academic, London 1991), p. 143.
- [18] J. N. Israelachvili, *J. Colloid Interface Sci.* **44**, 259 (1973).
- [19] R. G. Horn and D. T. Smith, *Appl. Opt.* **30**, 59 (1991).
- [20] G. Vigil, Z. Xu, S. Steinberg, and J. Israelachvili, *J. Colloid Interface Sci.* **165**, 367 (1994).
- [21] A. Berman, S. Steinberg, S. Campbell, A. Ulman, and J. Israelachvili, *Tribol. Lett.* **4**, 43 (1998).
- [22] Y. Golan, N. A. Alcantar, T. L. Kuhl, and J. Israelachvili, *Langmuir* **16**, 6955 (2000).
- [23] B. Xu, H. D. Wang, Y. Wang, G. Y. Zhu, Z. Li, and E. K. Wang, *Anal. Sci.* **16**, 1061 (2000).
- [24] The amplitude, u , was calculated as $u = Q / \pi d_{26} U_{el}$ with the Q factor $Q = f / (2\Gamma) = 6000$, the piezoelectric coefficient $d_{26} = 3.1$ pm/V, and the voltage across the electrodes $U_{el} = 170$ mV. The maximum lateral speed du/dt is equal to $2\pi fu$, where $f = 4$ MHz.
- [25] W. P. Mason, *Electromechanical Transducers and Wavefilters* (Van Nostrand, Princeton, 1948).
- [26] J. M. Levins and T. K. Vanderlick, *J. Colloid Interface Sci.* **185**, 449 (1997).
- [27] K. L. Johnson, K. Kendall, and A. D. Roberts, *Proc. R. Soc. London, Ser. A* **324**, 301 (1971).
- [28] R. G. Horn, J. N. Israelachvili, and F. Pribac, *J. Colloid Interface Sci.* **115**, 480 (1987).
- [29] D. Maugis, *J. Adhes. Sci. Technol.* **10**, 161 (1996); K. N. G. Fuller and D. Tabor, *Proc. R. Soc. London, Ser. A* **345**, 327 (1975); K. L. Johnson, in *The Mechanics of Contact between Deformable Solids*, edited by A. D. de Pater and J. J. Kalker (Delft University Press, Delft, 1976), pp. 26–40.
- [30] J. M. Levins and T. K. Vanderlick, *J. Phys. Chem.* **96**, 10405 (1992); *ibid.* **99**, 5067 (1995).
- [31] L. O. Heim, J. Blum, M. Preuss, and H. J. Butt, *Phys. Rev. Lett.* **83**, 3328 (1999).
- [32] K. L. Johnson, *Contact Mechanics* (Cambridge, New York, 1985).
- [33] C. Dominik, A. G. G. M. Tielens, *Philos. Mag. A* **72**, 783 (1995).
- [34] We used Eq. (15.25) in Ref. [17] with the parameters radius $R = 1$ cm, elastic modulus $K = 10$ GPa, and surface energy $W_{12} = 100$ mN/m to obtain an estimate of the order of magnitude.
- [35] D. Johannsmann, K. Mathauer, G. Wegner, and W. Kroll, *Phys. Rev. B* **46**, 7808 (1992).
- [36] While plastic subsurface deformation in principle could be viewed as a contribution to adhesion hysteresis, we define it as a distinct process here.
- [37] S. Berg and D. Johannsmann (unpublished).